PCCP

Accepted Manuscript

ROYAL SOCIETY OF CHEMISTRY

www.rsc.org/pccp

Correlation between the Surface Electronic Structure and CO-oxidation Activity of Pt Alloys

Hideki Abe,[†,§,] Hideki Yoshikawa,[†] Naoto Umezawa,[†,§] Ya Xu,[†] Govindachetty Saravanan,[†,⊤] Gubbala V. Ramesh,[†,*] Toyokazu Tanabe,[†] Rajesh Kodiyath,[†] Shigenori Ueda,[‡] Nobuaki Sekido,[†] Yoko Yamabe-Mitarai,[†] Masahiko Shimoda,[†] Takahisa Ohno,[†] Futoshi Matsumot[§§] and Takayuki Komatsu[§§§]*

† National Institute for Materials Science, 1-1 Namiki, Tsukuba, Ibaraki 305-0044, Japan

§ PRESTO, Japan Science and Technology Agency (JST), 4-1-8 Honcho Kawaguchi, Saitama 332-0012, Japan (PRESTO: Precursory Research for Embryonic Science and Technology)

⊤ CSIR-National Environmental Engineering Research Institute (CSIR-NEERI), Environmental Materials Division, Nehru Marg, Nagpur 440020, India

‡ NIMS Beamline Station at SPring-8, 1-1-1 Kouto, Sayo, Hyogo 679-5148, Japan

§§ Department of Material and Life Chemistry, Faculty of Engineering, Kanagawa University, 3-27-1, Rokkakubashi, Kanagawa-ku, Yokohama 221-8686, Japan

§§§ Department of Chemistry and Materials Science, Tokyo Institute of Technology 2-12-1-E1-10 Ookayama, Meguro-ku, Tokyo 185-8550, Japan

KEYWORDS

Alloy catalysts, CO oxidation, CO adsorption, surface electronic structure, *d*-band center

ABSTRACT

The surface electronic structure and CO-oxidation activity of Pt and Pt alloys, Pt_3T (T = Ti, Hf, Ta, Pt), were investigated. At temperatures below 538 K, the CO-oxidation activities of Pt and Pt_3T increased in the order Pt < Pt_3Ti < Pt_3Hf < Pt_3Ta. The center-of-gravity of the Pt *d*-band (the *d*-band center) of Pt and Pt_3T was theoretically calculated to follow the trend Pt_3Ti < Pt_3Ta < Pt_3Hf < Pt. The CO-oxidation activity showed a volcano-type dependence on the d-band center, where Pt_3Ta exhibited a maximum in activity. Theoretical calculations demonstrated that the adsorption energy of CO to the catalyst surface monotonically decreases with the lowering in the *d*-band center because of diminished hybridization of the surface *d*-band and the lowest-unoccupied molecular orbital (LUMO) of CO. The observed volcano-type correlation between the *d*-band center and the CO oxidation activity is rationalized in terms of the CO adsorption energy which counterbalances the surface coverage by CO and the rate of CO oxidation.

1. INTRODUCTION

The development of environmental-remediation technologies is of paramount importance to balance the growth in economy and the natural environment. One of the key objectives of the current environmental-purification technologies is reduction of expensive precious-group metals (PGMs: Pt, Pd and Rh) in automobile catalysts.[1,2] There have been numerous approaches to alloy PGMs and more abundant metals such as Ni or Co to achieve high performance and low materials costs (alloy catalysts).[3-7] However, it still remains a challenge to adequately design alloy catalysts for exhaust purification, because of the lack of understanding in correlation between the catalytic activity and experimentally measureable or theoretically calculable parameters of the alloys, such as a center-of-gravity of the Pt *d*-band (the *d*-band center).[8-14] Furthermore, surface segregation, which readily occurs on alloy surfaces in harsh conditions including high-temperature exhaust, makes it difficult to interrelate the apparent activity with the electronic and/or atomic structure of unperturbed surfaces.[15] To evaluate an inherent alloying effect on the exhaust-purification activity of alloy catalysts, it is required to investigate thermally stable alloys with high melting points (> 2000 K), such as early-*d*-Pt alloys (Pt-*T*: *T* = early *d*-metals), because their high ordering enthalpies can inhibit surface segregation and segregation-induced changes on the electronic or atomic structure of the surface.[16-18]

Here we report that a simple correlation can be established between the apparent exhaust-purification activity and the surface electronic structure of early-*d*-Pt alloys, Pt_3T (*T* = Ti, Ta of Hf). X-ray photoemission spectroscopy using synchrotron radiation (Hard X-ray Photoemission Spectroscopy: HX-PES) demonstrated that the surface of Pt_3T was free from segregation when exposed to a simulated exhaust (a 2:1 mixture of carbon monoxide (CO) and O_2 gases, 10 kPa) at temperatures below 598 K. At temperatures lower than 538 K, the catalytic activity of Pt and

Pt_3T for the oxidation of CO increased in the order Pt < Pt_3Ti < Pt_3Hf < Pt_3Ta. This trend leads to a volcano-type dependence of the CO oxidation activity on the theoretically calculated center-of-gravity of the Pt *d*-band (the *d*-band center) which increases in the order Pt < Pt_3Hf < Pt_3Ta < Pt_3Ti. Theoretical calculations have further demonstrated that the adsorption energy of CO to the catalyst surface monotonically decreases with the lowering in the *d*-band center because of diminished hybridization of the surface *d*-band and the lowest-unoccupied molecular orbital (LUMO) of CO. The observed volcano-type correlation between the *d*-band center and the CO oxidation activity is accounted for in terms of the CO adsorption energy which counterbalances the surface coverage by CO and the rate of CO oxidation. This established correlation allows us to understand and even predict the exhaust-purification activity of unknown Pt-based alloys by theoretically calculating and/or experimentally determining the d-band center, which will be a guiding principle in the quest for efficient alloy catalysts for exhaust purification.

2. EXPERIMENTAL SECTION

2.1 Sample preparation.

Polycrystalline samples of intermetallic Pt_3T (T = Ti, Ta, and Hf) were synthesized in a pure Ar atmosphere (99.9999 %) with an arc furnace. Prior to the synthesis, the arc furnace was evacuated to a vacuum level with a pressure lower than 10^{-3} Pa and backfilled with pure Ar. All starting materials were purchased from Furuya Kinzoku Co. An aliquot of 1 g of Pt powder (99.9 %) was pelletized with a stainless-steel die and melted with the arc furnace into an ingot. Titanium (sponge, 99 %) and Ta (wire, 99 %) metals were used as received. As-purchased Hf metal (chunk, 98 %) was first melted with the arc furnace to remove surface oxides. The ingots of Pt and the other metals were weighed such that the molar ratio was Pt:T = 3:1 and melted together in the arc furnace. The ingot obtained, with a combined weight of approximately 3 g, was cut into two halves with a diamond saw. One of the halves was ground with an agate mortar for powder X-ray diffraction (*p*XRD), Brunauer–Emmett–Teller (BET) surface area measurements and catalytic CO oxidation measurements. Slices that were 0.5 mm thick were cut from the other half and polished to a mirror finish for hard X-ray photoemission spectroscopy (HX-PES) measurements.

2.2 Characterization.

*p*XRD (RIGAKU RINT 2000, Cu-Kα radiation, λ = 1.541 Å) was used to examine the powdered samples of the Pt_3T alloys. The specific surface area of each sample was determined using the BET method. A Micromeritics ASAP 2020 was used to collect a partial adsorption isotherm at liquid-nitrogen temperature (77 K) using krypton as the adsorption gas. HX-PES was performed at room temperature under ultra-high vacuum using synchrotron radiation (5.95 keV, SPring-8, beamline BLXU15) and an electron energy analyzer (VG SCIENTA R4000).[19] A 0.3 mm-thick

Pt plate (99.9 %, Furuya Kinzoku Co.), a 0.3 mm-thick Ti plate (99.9 %, Nilaco Co.) and slices of Ta and Hf taken from button-shaped ingots prepared in the arc furnace were used as references for HX-PES. All samples for HX-PES were fixed with carbon adhesives to grounded Cu sample holders. The HX-PES data were referenced to the Fermi edge of an Au film that was electrically connected to the samples via the sample holder.

2.3 Catalytic measurements.

A fixed-bed flow micro-reactor (Ohkura Riken) equipped with a gas chromatograph (GL Sciences) was used to evaluate the catalytic activities of the samples for the oxidation of CO.[20] An aliquot of 150 mg of Pt or Pt_3T powder was introduced in the micro-reactor and subjected to a constant flow (100 ml min^{-1}) of a reactant gas that consisted of CO, O_2 and He at a molar ratio of 2:1:97 (Sumitomo Seika Chemicals). The BET surface areas of the powders were determined prior to the catalytic measurements. The composition of the outlet gas from the micro-reactor was analyzed at different sample temperatures ranging from 473 to 573 K.

2.4 Theoretical calculations.

Theoretical calculations of the electronic structures of the catalyst were performed using density-functional theory. The exchange-correlation energy functional was represented by the Perdew–Bruke–Ernzerhof[21] generalized gradient approximation. Projector-augmented wave pseudopotentials were employed as implemented in the VASP code.[22,23] The valence configurations of the pseudo-potentials were $5d^9 6s^1$ for Pt, $3p^6 3d^3 4s^1$ for Ti, $5p^6 5d^3 6s^2$ for Ta and $5p^6 5d^2 6s^2$ for Hf. The energy cutoff for the plane-wave basis set expansion was set at 500 eV. Monkhorst–Pack *k*-point sets of 12×12×12 and 10×10×10 were used for the 1-atom and 4-atom unit cells for Pt and Pt_3Ti, respectively, whereas an 8×8×8 set was used for the 16-atom unit cells of Pt_3Ta and Pt_3Hf. The optimized lattice constants were as follows: a = 3.98 Å for Pt; a = 3.95

Å for Pt_3Ti; a = 4.93 Å, b = 5.61 Å, c = 9.40 Å, β = 100.56° for Pt_3Ta; and a = 5.71 Å, b = 5.71 Å, c = 9.32 Å, γ = 119.99° for Pt_3Hf, using the reported crystallographic parameters.[24-26]

The unit cells were extended for the creation of slab models of the Pt(111), Pt_3Ti(111), Pt_3Ta(001) and Pt_3Hf(001) surfaces. The Pt(111) slab model consisted of 15 layers of Pt planes, including 120 atoms in total, and a vacuum of the same thickness as the Pt slab. The 7-9th layers were fixed during the surface relaxations to represent the bulk region. The 120-atom slab model of Pt_3Ti(111) was created in the same manner as that of Pt(111). The Pt_3Ta(001) slab model consisted of 12 layers of Pt_3Ta planes, including a total of 96 atoms, and a vacuum of the same thickness as the Pt_3Ta slab. The 5-8th layers were fixed during the surface relaxations. A similar model was constructed for the Pt_3Hf(001) surface. For the surface calculations, the *k*-point sampling was set at 2×2×1. The atomic positions of the slab modes were fully relaxed except for the fixed layers. The total density of states (DOS) was plotted with a smearing factor of 0.05 eV. The *d*-band centers were evaluated by applying the following formula to the calculated DOS:

$$d\text{-band center} = \frac{\int E\ \mathrm{DOS}(E)dE}{\int \mathrm{DOS}(E)dE}$$

Where DOS(E) is the density of states of the occupied *d*-states.

For the calculation of the CO adsorption energy on each surface, a CO molecule was placed above a Pt atom with the C–Pt distance fixed at 1.94 Å (Figure S1).[27] The total energy of a single CO molecule, E_{tot}(CO), was also computed using the same size supercell to evaluate the CO adsorption energy according to

$E_{ads} = E_{tot}$(CO-Metal) – E_{tot}(Metal) – E_{tot}(CO),

where E_{tot}(CO-Metal) and E_{tot}(Metal) are the total energies of the slabs with or without a CO molecule on the surface, respectively.

3. Results and Discussion

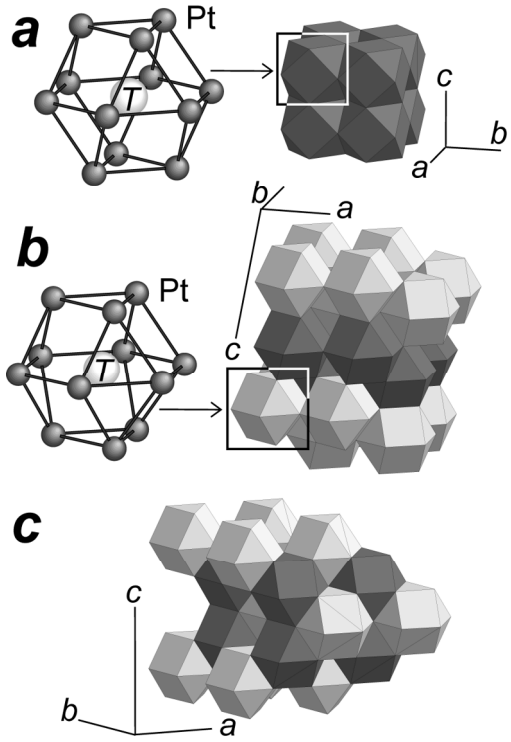

Figure 1. Crystal structures of Pt and Pt_3T. *a*. Ball-and-stick model for a $Pt_{12}T$ cubo-octahedron (left) and the crystal structures of Pt and Pt_3Ti as a polygonal model (right). The grey polyhedra correspond to the $Pt_{12}Pt$ and/or $Pt_{12}T$ cubo-octahedra. *b*. Ball-and-stick model for a structural derivative of the $Pt_{12}T$ cubo-octahedron (left) and a polygonal model for Pt_3Ta (right). The grey and white polyhedra correspond to the cubo-octahedral $Pt_{12}T$ and its structural derivative, respectively. *c*. Polygonal model for Pt_3Hf.

Figure 1 presents the structural models for Pt and Pt_3T: Pt, $Fm\bar{3}m$, a = 3.9200 Å; Pt_3Ti, Cu_3Au type, $Pm\bar{3}m$, a = 3.9040 Å; Pt_3Ta, Pt_3Nb type, $P2_1/m$, a = 4.8690 Å, b = 5.5370 Å, c = 9.2690 Å,

β = 100.62°; and Pt_3Hf, Ni_3Ti type, $P6_3/mmc$, a = 5.6360 Å, c = 9.2080 Å, β = 120°.[24-26] The Pt and/or $Pt_{12}Ti$ cubo-octahedron depicted by the stick-and-ball model and grey polyhedra in Figure 1*a* share the six square planes of the neighboring polyhedra in forming the framework of Pt and/or Pt_3Ti. The crystal structures of Pt_3Ta and Pt_3Hf, unlike that of either Pt or Pt_3Ti, are constructed from two types of $Pt_{12}T$ polyhedra with different configurations (Figure 1*b* and 1*c*). One of the two types of $Pt_{12}T$ polyhedra is isomorphic with the $Pt_{12}Ti$ cubo-octahedron. The other type of $Pt_{12}T$ polyhedron, which is depicted by a stick-and-ball model and white polyhedra, is a structural derivative obtained by rotating one of the eight Pt triangles of a $Pt_{12}T$ cubo-octahedron by 180°. The monoclinic structure of Pt_3Ta is constructed by face- and edge-sharing of the $Pt_{12}T$ cubo-octahedron and its structural derivative. The hexagonal structure of Pt_3Hf is also constructed by face- and ledge-sharing of the two types of $Pt_{12}T$ polyhedra, but in a different sequence (Figure 1*c*).

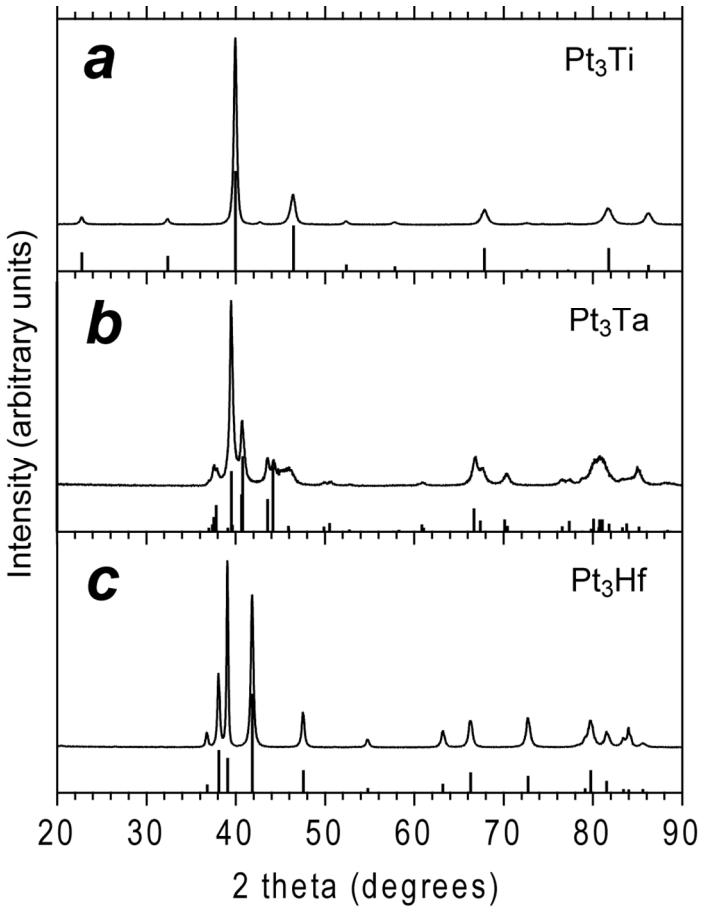

Figure 2. *p*XRD profiles for Pt_3Ti (*a*), Pt_3Ta (*b*) and Pt_3Hf (*c*). Simulated diffraction patterns are indicated as solid bars.

Figure 2 shows the *p*XRD profiles for Pt_3T, together with the diffraction patterns simulated using the reported crystallographic parameters. The *p*XRD profiles for Pt_3Ti, Pt_3Ta and Pt_3Hf are consistent with the simulated patterns. The synthesized samples of Pt_3T were single-phase ordered alloys with the desired compositions and crystal structures.

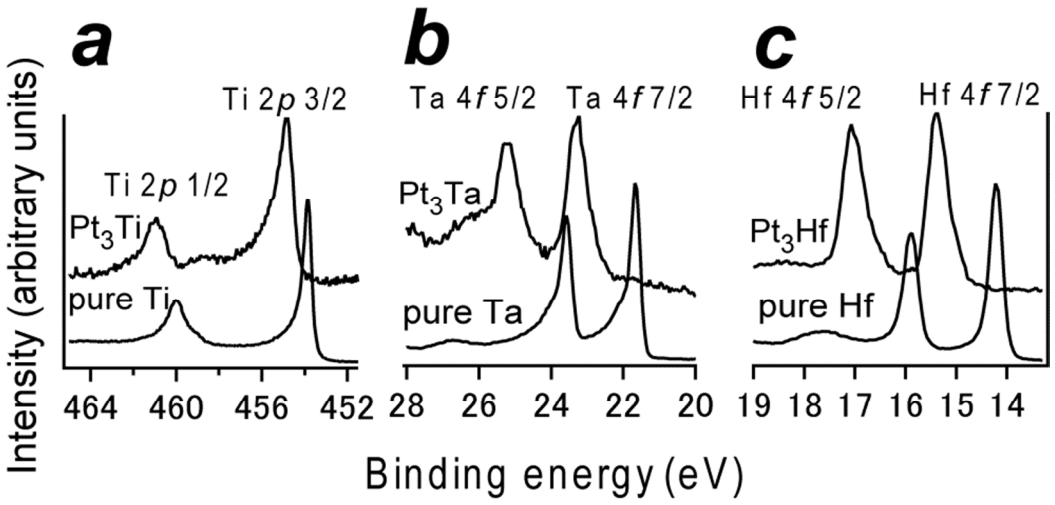

Figure 3. HX-PES profiles for the core levels of the *T* elements in Pt_3T. *a*. Ti 2*p* levels of Pt_3Ti and pure Ti. *b*. Ta 4*f* levels of Pt_3Ta and pure Ta. *c*. Hf 4*f* levels of Pt_3Hf and pure Hf.

Figure 3 shows the HX-PES profiles for the core levels of the *T* elements in Pt_3T. The Ti 2*p* levels of Pt_3Ti were shifted by 1.0 eV toward high binding energies relative to those of pure Ti (Figure 3*a*). Similar shifts were observed for the other Pt_3T (Figures 3*b* and 3*c*). Both the Ta 4*f* levels of Pt_3Ta and the Hf 4*f* levels of Pt_3Hf were shifted by 1.5 eV toward high binding energies relative to those of the corresponding pure metals (Table 1).

Table 1. Core Levels of the *T* Elements in Pt_3T

Material	Binding energy (eV)	Binding energy (eV)	spin-orbit splitting Δ^a (eV)
	Ti $2p_{3/2}$	Ti $2p_{1/2}$	
Pt_3Ti	454.82±0.20 (455.2)[b]	460.92±0.20 (461.3)[b]	6.10
Ti	453.82±0.20 (454.0)[c]	460.02±0.20 (460.0)[c]	6.20
	Ta $4f_{7/2}$	Ta $4f_{5/2}$	
Pt_3Ta	23.22±0.20	25.27±0.20	2.05
Ta	21.67±0.20 (21.7)[d]	23.57±0.20 (23.7)[d]	1.90
	Hf $4f_{7/2}$	Hf $4f_{5/2}$	
Pt_3Hf	15.37±0.20	17.07±0.20	1.70
Hf	14.22±0.20 (14.31)[e]	15.87±0.20 (15.98)[e]	1.65 (1.67)[e]

Note: Literature values are indicated in parentheses.

a. Δ: spin-orbit splitting.

b. ref. 28-30.

c. ref. 31,32.

d. ref. 33,34.

e. ref. 35.

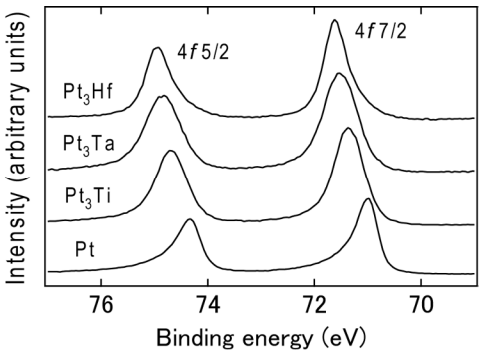

Figure 4. HX-PES profiles for the Pt core levels of pure Pt and Pt_3T.

The HX-PES profiles for the Pt 4*f* levels of pure Pt and Pt_3T are presented in Figure 4. The Pt $4f_{7/2}$ and $4f_{5/2}$ levels were, in descending order, Pt, Pt_3Ti, Pt_3Ta and Pt_3Hf, where the amplitude of the spin-orbit splitting was 3.35±0.20 eV irrespective of the identity of *T* (Table 2). In summary, the synthesized Pt_3T samples were ordered alloys that exhibited different crystal structures and electronic structures from those of the constituent elements.

Table 2. Pt Core Levels of Pure Pt and Pt_3T

Material	Pt $4f_{7/2}$ binding energy (eV)	Pt $4f_{5/2}$ binding energy (eV)	spin-orbit splitting Δ^a (eV)
Pt	70.97±0.20 (71.30)[b]	74.32±0.20 (74.23)[b]	3.35
Pt_3Ti	71.37±0.20 (71.3)[c]	74.72±0.20 (74.65)[c]	3.35
Pt_3Ta	71.52±0.20	74.82±0.20	3.30
Pt_3Hf	71.62±0.20	74.92±0.20	3.30

a. Δ: spin-orbit splitting.

b. ref. 36.

c. ref. 28-30.

Prior to the catalytic testing, the chemical stability of each Pt_3T surface was examined at elevated temperatures in a reactant gas that consisted of CO, O_2 and He at a molar ratio of 2:1:97. Each Pt_3T surface was exposed to the reactant gas for 1 hour in a fixed-bed flow micro-reactor at a temperature of 548, 598 or 823 K. After exposure to the reactant gas, the Pt_3T samples were transferred to the UHV chamber for HX-PES measurements.

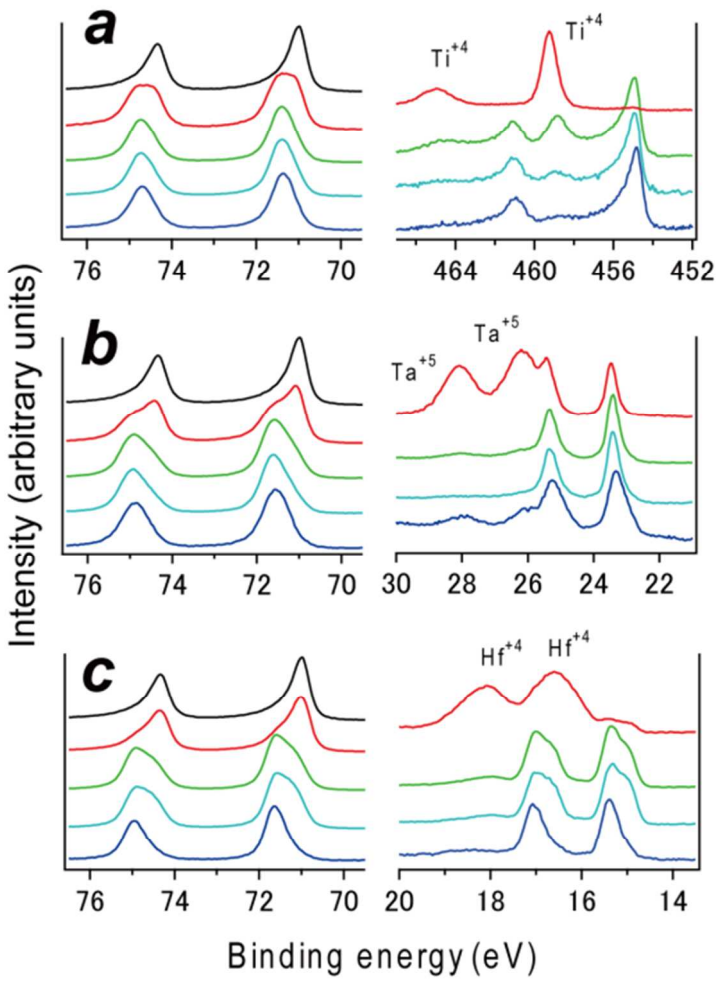

Figure 5. HX-PES profiles for the Pt_3T surfaces subjected to different atmospheres. *a*. Pt 4*f* (left) and Ti 2*p* levels (right) of the Pt_3Ti surface. *b*. Pt 4*f* (left) and Ta 4*f* levels (right) of the Pt_3Ta surface. *c*. Pt 4*f* (left) and Hf 4*f* levels (right) of the Pt_3Hf surface. Colored profiles correspond to

the as-prepared surfaces (blue) and to the surfaces heated in the reactant gas at 548 K (light blue), 598 K (green) or 823 K (red). Black profiles indicated in the left panels from *a.* through *c.* correspond to the Pt 4*f* levels of the pure Pt surface.

The left panel of Figure 5*a* shows Pt 4*f* profiles for the Pt_3Ti surfaces subjected to different atmospheres. Both of the Pt 4*f* profiles for the Pt_3Ti surfaces heated at 548 K (light-blue profile) or 598 K (green profile) were identical to that for the as-prepared Pt_3Ti surface (blue profile). The Pt 4*f* emission peaks for the Pt_3Ti surface heated at 823 K (red profile), however, exhibited large shoulders at 71.02±0.20 and 74.36±0.20 eV. These values were consistent with the Pt 4*f* emission peaks for the pure Pt surface at 70.97±0.20 and 74.32±0.20 eV, respectively (black profile). The Pt_3Ti surface, when heated to 823 K in the reactant gas mixture, precipitated pure Pt.

The right panel of Figure 5*a* shows the Ti 2*p* profile for the Pt_3Ti surfaces. The Ti $2p_{3/2}$ (454.87±0.20 eV) and Ti $2p_{1/2}$ (460.97±0.20 eV) levels of the as-prepared surface were consistent with those of the surfaces heated at 548 K or 598 K, though an additional peak was observed at 458.85±0.20 eV for the heated surfaces. This peak was attributed to the adsorption of oxygen to the surface Ti to form a suboxide, TiO_{2-x} ($x > 0$).[28-30, 37] For the sample heated at 823 K, the Ti emission peaks for Pt_3Ti and TiO_x ($x < 2$) nearly vanished. Two peaks appeared at 459.25±0.20 and 465.00±0.20 eV instead, corresponding to the Ti $2p_{3/2}$ and Ti $2p_{1/2}$ emissions, respectively, from titanium dioxide, $Ti^{4+}O_2$.[31,32] The Pt_3Ti surface retained its chemical composition when heated in the reactant gas at temperatures below 598 K but was decomposed at 823 K into pure Pt and TiO_2.

The left and right panels of Figure 5*b* show the Pt 4*f* and Ta 4*f* profiles, respectively, for the Pt_3Ta surfaces. The Pt 4*f* profiles for the Pt_3Ta surfaces heated at 548 or 598 K were virtually identical to that of the as-prepared surface (left panel) and the Ta 4*f* profiles for the Pt_3Ta

surfaces heated at 548 or 598 K were similar to that for the as-prepared surface (right panel). A shoulder at 26.0 eV and a weak peak at 28.0 eV on the Ta 4*f* profile for the as-prepared Pt_3Ta surface (blue profile in the right panel) correspond to a surface contamination that was removed by heating in the reactant gas. The Pt_3Ta surface retained the chemical composition of the as-prepared surface when heated to temperatures ranging from 548 to 598 K. At a temperature of 823 K, the emission peaks that correspond to pure Pt (red profile in the left panel) and $Ta^{5+}{}_2O_5$ (red profile in the right panel) became clearly visible.[33,34] At 823 K, the Pt_3Ta surface decomposed into pure Pt and Ta_2O_5, similar to the behavior of the Pt_3Ti surface.

The left and right panels of Figure 5*c* show the Pt 4*f* and Hf 4*f* profiles for the Pt_3Hf surface. The Pt emission peaks for the surfaces heated to 548 K or 598 K, 71.60±0.20 and 74.90±0.20 eV, respectively, were consistent with those observed for the as-prepared Pt_3Hf surface, at 71.62±0.20 and 74.92±0.20 eV, respectively (left panel). The Hf emission peaks for the surfaces heated at 548 K or 598 K, 15.35±0.20 and 17.00±0.20 eV, respectively, were also consistent with those for the as-prepared Pt_3Hf surface, 15.37±0.20 and 17.07±0.20 eV, respectively (right panel).

The Pt 4*f* and Hf 4*f* emission peaks for the Pt_3Hf surfaces heated at 548 or 598 K, unlike those for the as-prepared surface, exhibited shoulders at lower binding energies. The binding energies for the shoulders of the Pt 4*f* emission peaks were revealed by deconvolution to be at 71.15±0.20 and 74.46±0.20 eV. These values were not consistent with the Pt 4*f* levels of the pure Pt surface, 70.97±0.20 and 74.32±0.20 eV. The binding energies for the shoulders of the Hf 4*f* emission peaks, 14.98±0.20 and 16.66±0.20 eV, were also inconsistent with the values for HfO_2 (16.60±0.20 and 18.10±0.20 eV), Pt_3Hf (15.37±0.20 and 17.07±0.20 eV) or pure Hf (14.22±0.20 and 15.87±0.20 eV).[35]

Morant et al. reported that a suboxide of Hf, HfO_{2-x} ($x > 0$), was formed on a Hf surface at room temperature at an early stage of adsorption of oxygen ($\leq$ 5 L).[35] The reported binding energies for the Hf 4*f* emissions from HfO_{2-x}, 15.1 and 16.8 eV, are similar to the values for the shoulders of the Hf 4*f* emissions from Pt_3Hf surfaces heated at 548 or 598 K, 14.98±0.20 and 16.66±0.20 eV, respectively. The observed shoulders of the Hf 4*f* peaks for the Pt_3Hf surfaces heated at 548 or 598 K are assigned to a suboxide of the surface Hf that may accompany a core-level shift for the surface Pt.

The Pt 4*f* profile for the Pt_3Hf surface heated at 823 K (red profile in the left panel of Figure 5*c*) was different from that for the surface heated at either 548 or 598 K and was similar to that for the pure Pt surface. The Hf 4*f* profile for the surface heated at 823 K (red profile in the right panel of Figure 5*c*) showed two peaks that corresponded to $Hf^{4+}O_2$ at 16.60±0.20 and 18.10±0.20 eV. The Pt_3Hf surface retained the chemical composition of the as-prepared surface when heated to temperatures ranging from 548 to 598 K but decomposed into pure Pt and HfO_2 when heated at 823 K.

Summarizing the HX-PES data in the core-level region, we conclude that the Pt_3T surfaces retain their chemical compositions when exposed to the O_2-containing reactant gas, as long as the temperature is lower than 598 K. When the temperature exceeds 823 K, the Pt_3T surfaces decomposed into pure Pt and a transition-metal oxide of *T* in its highest available oxidation state. Indeed, the O1*s* emission peaks for the Pt_3T surfaces heated at 823 K were more intense than those for the surfaces heated below 598 K (see supporting information, Figure S2). Catalytic tests were performed at temperatures below 598 K to establish a reliable correlation between the catalytic activity and the surface electronic structure of Pt_3T.

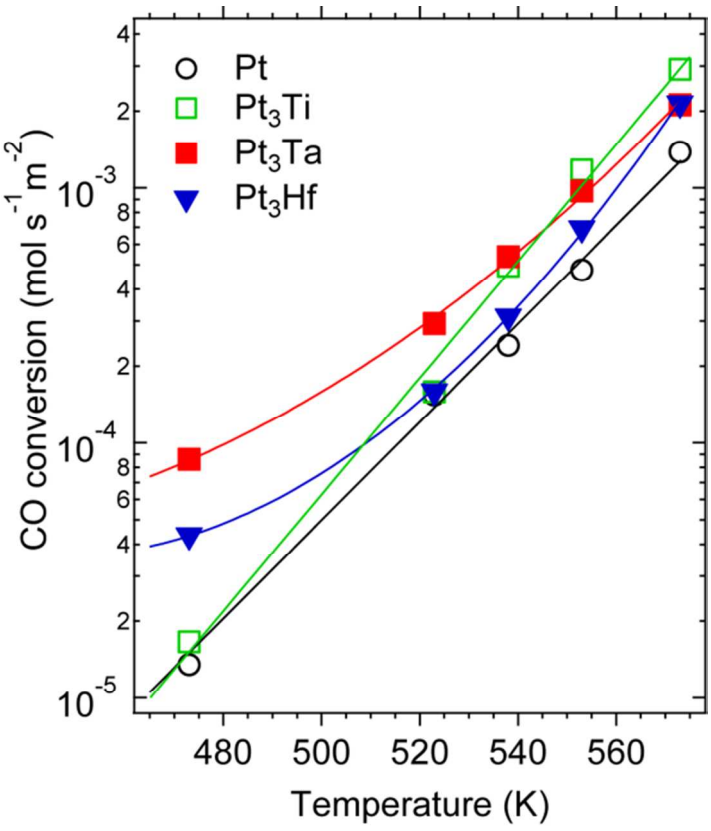

Figure 6. Catalytic CO oxidation over the Pt and Pt_3T surfaces. The specific activities for CO oxidation over Pt (○), Pt_3Ti (□), Pt_3Ta (■) and Pt_3Hf (▼) are plotted as functions of temperature.

Figure 6 shows the temperature dependence of the catalytic activities of Pt and Pt_3T toward the oxidation of CO. The specific CO oxidation activity of Pt increased monotonically with increasing temperature (open circles in Figure 6). The specific CO oxidation activities of Pt at 473 and 573 K were 1.35×10^{-5} and 1.38×10^{-3} $mols^{-1}m^{-2}$, respectively. The specific CO oxidation activity of Pt_3Ti also increased with increasing temperature but at a higher rate. The specific activity of Pt_3Ti at 473 K was 1.66×10^{-5} $mols^{-1}m^{-2}$, which was higher than the value of Pt at the same temperature. At 573 K, however, the specific activity of Pt_3Ti was 2.91×10^{-3} $mols^{-1}m^{-2}$, which was double that observed for Pt. Pt_3Ta showed the highest specific CO oxidation activity at low temperatures. The specific activity of Pt_3Ta at 473 K, 8.62×10^{-5} $mols^{-1}m^{-2}$, was 5-fold

higher than the values for Pt or Pt_3Ti. The specific activity of Pt_3Hf at each temperature was between those of Pt_3Ta and Pt. The specific CO oxidation activities of Pt and Pt_3T were Pt < Pt_3Ti < Pt_3Hf < Pt_3Ta at temperatures below 538 K and Pt < Pt_3Hf < Pt_3Ta < Pt_3Ti above 538 K.

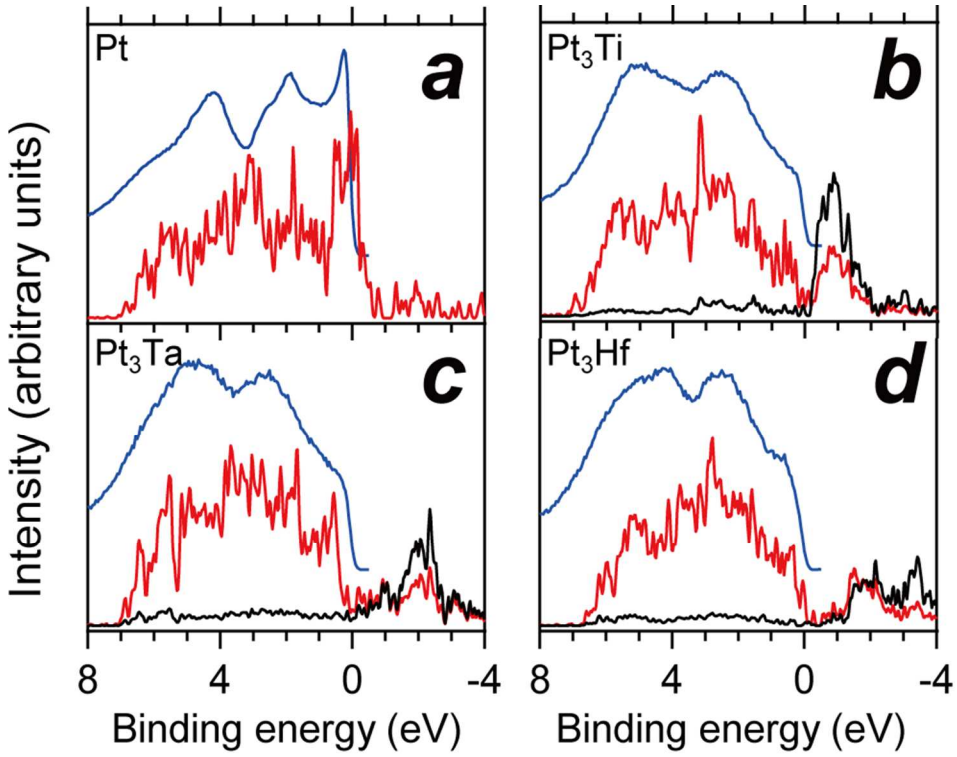

Figure 7. HX-PES profiles and calculated density-of-states (DOS) for Pt and Pt_3T in the valence region. *a*. Pt. *b*. Pt_3Ti. *c*. Pt_3Ta. *d*. Pt_3Hf. The blue, red and black profiles correspond to the experimental HX-PES data and the DOS components of Pt and *T*, respectively.

Figure 7 shows the HX-PES profiles for the pure Pt and the as-prepared Pt_3T surfaces in the valence region, together with the calculated DOS for Pt and *T*. Both the HX-PES and the DOS profiles for pure Pt exhibit a large peak immediately below the Fermi level, assigned to the Pt 5*d* orbital (Figure 7*a*). In contrast, the HX-PES profile for Pt_3Ti exhibits no corresponding peak below the Fermi level (Figure 7*b*). Theoretical calculations have shown that the Pt 5*d* and Ti 3*d* orbitals are hybridized to split into anti-bonding and bonding states located above and below the

Fermi level.[38] The valence band of Pt_3Ti is a bonding state of Pt and Ti that consists mostly of the Pt 5*d* state with a small Ti 3*d* component. As with Pt_3Ti, neither Pt_3Ta (Fig. 7*c*) nor Pt_3Hf (Figure 7*d*) shows any predominant peaks immediately below the Fermi level in the HX-PES or DOS profiles: the Ta 5*d* orbital and the Hf 5*d* orbital are hybridized with the Pt 5*d* orbital and split into anti-bonding and bonding states.

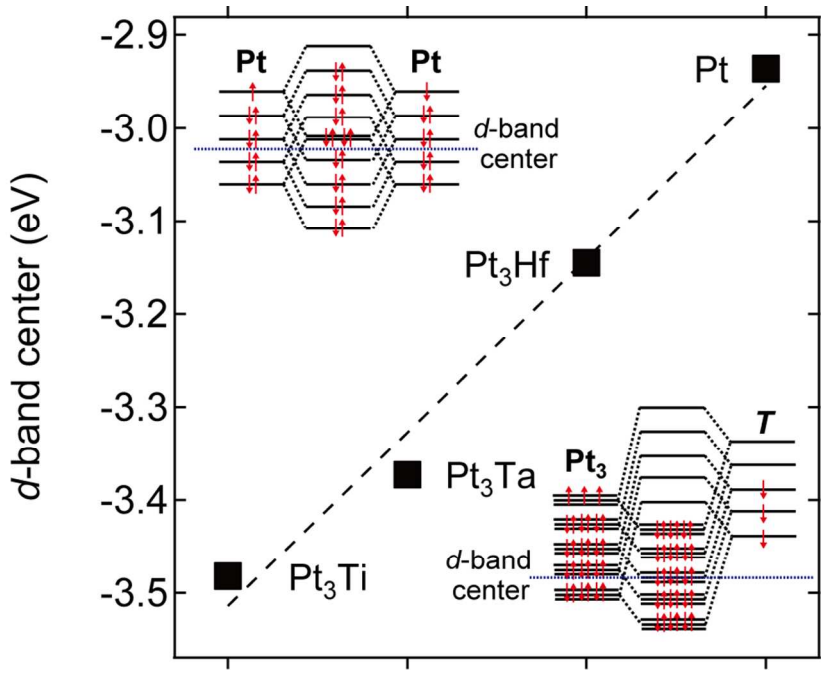

Figure 8. Calculated *d*-band centers for Pt and Pt_3T. Insets show schematic energy diagrams for Pt (top left) and Pt_3T (bottom right).

The calculated gravity centers of the filled Pt *d*-band (*d*-band center) for Pt and Pt_3T were ordered as Pt_3Ti < Pt_3Ta < Pt_3Hf < Pt (Figure 8). Pure Pt has the highest energy *d*-band center because the *d*-band in pure Pt is mostly filled by electron pairs, as shown in the top-left inset. In Pt_3T, however, few electrons are donated by the *T* element, and only the bonding states are occupied, which results in a downshift in the *d*-band center (bottom-right inset). The energy level of the *d*-band center of Pt_3T is determined by the energy gap between the *d*-orbitals of Pt and *T*: a smaller energy gap results in a lower *d*-band center due to a larger energy splitting. The energy

levels of the *d*-orbitals were calculated as -5.52 eV (Pt), -4.12 eV (Ti), -3.55 eV (Ta), and -2.64 eV (Hf). These values are consistent with the trend presented in Figure 8.

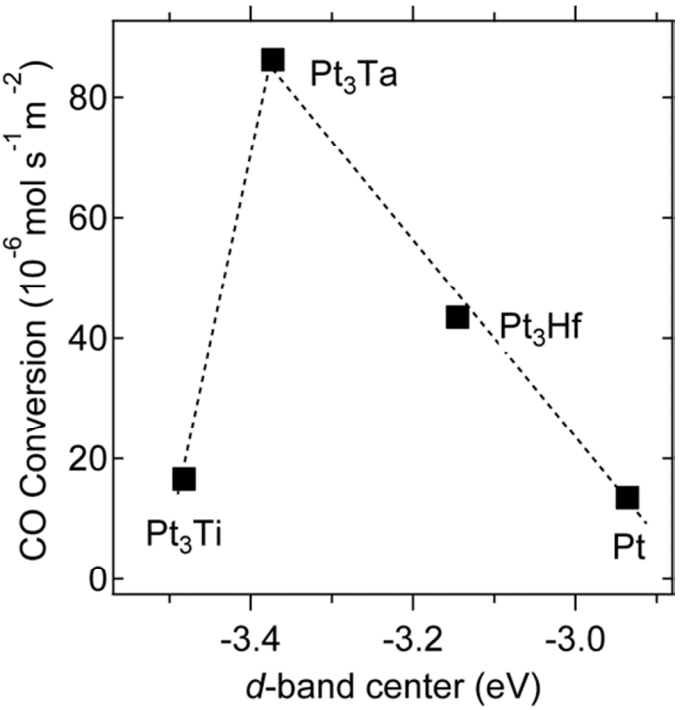

Figure 9. Correlation between the CO oxidation activity and the *d*-band center. Specific CO oxidation activities of Pt and Pt_3T at 473 K are plotted as a function of the *d*-band center.

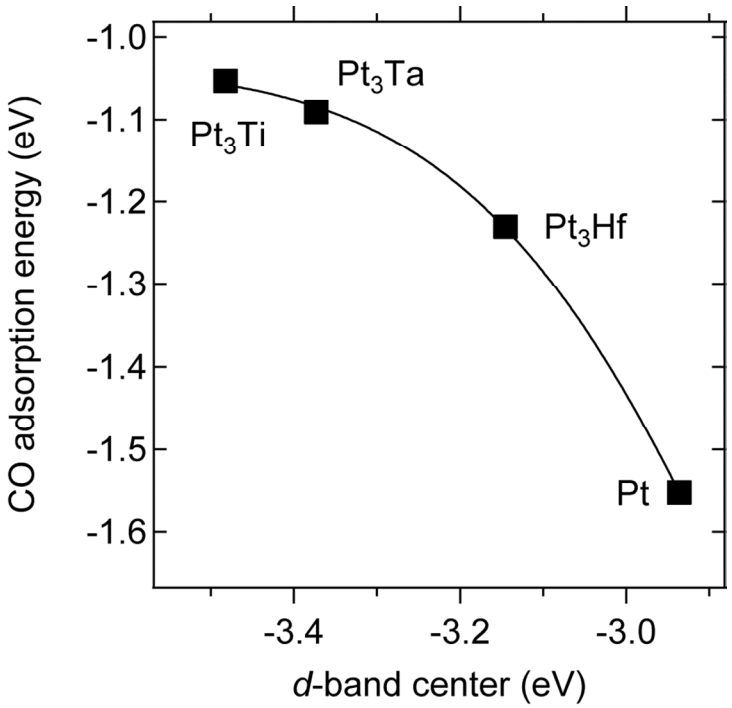

Figure 10. Correlation between the CO adsorption energy and the *d*-band center.

The CO oxidation activities at the lowest temperature in the measurement range, 473 K, were plotted against the calculated *d*-band centers (Figure 9). The CO oxidation activity exhibited a volcano-type dependence on the *d*-band center with Pt_3Ta at the top. The CO oxidation activities of Pt_3Ti and Pt_3Hf were higher than that of pure Pt, but lower than that of Pt_3Ta.

Figure 10 shows the theoretically calculated CO adsorption energy on the catalyst surface of Pt and Pt_3T. The amplitude of CO adsorption energy decreases monotonically as the *d*-band center decreases. The CO adsorption energy on the Pt_3Ti surface is 30 % lower than that on the pure Pt surface. This trend is attributed to poor electron back-donation from the Pt_3T sur-faces to CO admolecules, which is caused by the increased energy gap between the *d*-band center and the lowest unoccupied $2\pi^*$ molecular orbital (LUMO) of the CO admolecules.[27,39,40]

The volcano-type correlation established in this work may be assigned to a downshift in the *d*-band center of Pt_3T relative to that of Pt, which is accompanied by a weakening of the CO

adsorption. The CO adsorption to the Pt surface is so strong that the catalysis is blocked by the CO adlayer. In contrast, CO oxidation is poorly promoted by Pt_3Ti at low temperatures because CO admolecules readily desorb from the surface.[41-45] Pt_3Ta, which exhibits an intermediate *d*-band center, achieves the highest CO oxidation activity because of an optimum balance in the adsorption and desorption of CO.

CONCLUSIONS

In conclusion, we have demonstrated that ordered early *d*-metal alloys, Pt_3T (T = Ti, Ta and Hf), exhibit catalytic activities that are superior to that of pure Pt for the oxidation of CO. The specific CO oxidation activities of Pt and Pt_3T showed a volcano-type correlation with the *d*-band center of the catalyst. The observed volcano-type correlation has been interpreted as a result of the weakening of CO adsorption to the catalyst surface caused by a downshift in the *d*-band center of Pt_3T relative to that of Pt.

Outstanding issues and potential limitations to be addressed include the chemical composition of the catalyst surface at work, the surface dynamics of the reaction intermediates and how the atomic arrangement on the surface affects the apparent activity. The Pt_3Ta catalyst, which exhibited a very high CO oxidation activity, should be synthesized in the form of nanoparticles for practical use. These issues are challenging, yet worthy of effort, because the high activity and the reduced precious-metal content of alloy catalysts will strongly promote the future development of such metal catalysts for environmental and/or energy applications.

ASSOCIATED CONTENT

Supporting Information.

HX-PES profiles in the O1s and Pt $4p_{3/2}$ regions for the surfaces of Pt_3Ti, Pt_3Ta and Pt_3Hf that were heated at different temperatures in the reactant gas. This material is available free of charge via the Internet at http://pubs.acs.org.

Corresponding author

Hideki Abe, Ph.D. Tel: +81-29-860-4806; Fax: +81-29-859-2301
E-mail: ABE.Hideki@nims.go.jp
Gubbala V. Ramesh, Ph.D. E-mail: GUBBALA.Venkataramesh@nims.go.jp

ACKNOWLEDGMENT

This work was supported by the JST PRESTO program. We gratefully acknowledge Toyota Motor Corporation for financial support. The HX-PES measurements were performed under the approval of the NIMS Beamline Station (Proposal No. 2009B4608 and 2010A4609). The authors are grateful to HiSOR, Hiroshima University, and JAEA/SPring-8 for the development of HX-PES at BL15XU of SPring-8.

REFERENCES

(1) X. Xie, Y. Li, Z. Q. Liu, M. Haruta and W. Shen, *Nature*, 2009, **458**, 746-749.

(2) C. H. Kim, G. Qi and W. L. Dahlberg, *Science,* 2010, **327**, 1624-1627.

(3) S. Zhou, B. Varughese, B. Eichhorn, G. Jackson and K. Mcilwrath, *Angew. Chem. Int. Ed.*, 2005, **44**, 4539–4543.

(4) Y. Kang and C. Murray. *J. Am. Chem. Soc.* 2010, **132**, 7568–7569.

(5) J. L. Zhang, M. B. Vukmirovic, Y. Xu, M. Mavrikakis and R. R. Adzic, *Angew. Chem., Int. Ed.*, 2005, **44**, 2132–2145.

(6) V. R. Stamenkovic, B. S. Mun, K. J. J. Mayrhofer, P. N. Ross and N. M. Marković, *J. Am. Chem. Soc.* 2006, **128**, 8813–9.

(7) T. Komatsu and A. Tamura, *J. Catal.* 2008, **258**, 306–314.

(8) E. Nikolla, J. Schwank and S. Linic, *J. Am. Chem. Soc.* 2009, **131**, 2747-2754.

(9) T. Hofmann, T. H. Yu, M. Folse, L. Weinhardt, M. Bar, Y. Zhang, B. V. Merinov, D. J. Myers, W. A. Goddard III and C. Heske, *J. Phys. Chem. C* 2012, **116**, 24016-24026.

(10) F. Abild-Pedersen, A. Nilsson and J. K. Nørskov, *J. Phys. Chem. C* 2013, **117**, 6914-6915., and references therein.

(11) V. R. Stamenkovic, B. S. Mun, M. Arenz, K. J. J. Mayrhofer, C. A. Lucas, G. F. Wang, P. N. Ross and N. M. Marković, *Nature Mater.* 2007, **6**, 241-247.

(12) B. Hammer and J. K. Nørskov, *Nature* 1995, **376**, 238-240.

(13) Y. Morikawa, J. J. Mortensen, B. Hammer and J. K. Nørskov. *Surface Science*, 1997, **386**, 67-72.

(14) "Theory of adsorption and surface reactions"**,** B. Hammer and J. K. Nørskov, Kluwer Academic Publishers, 1997.

(15) C. A. Menning and J. G. G. Chen. *J. Chem. Phys.* 2009, **130**, 174709 (1-7).

(16) G. Saravanan, H. Abe, Y. Xu, N. Sekido, H. Hirata, S. Matsumoto, H. Yoshikawa and Y. Yamabe-Mitarai, *Langmuir* 2010, **26**, 11446–11451.

(17) H. Abe, F. Matsumoto, L. R. Alden, S. C. Warren, D. H. Abruña and F. J. DiSalvo, *J. Am. Chem. Soc.* 2008, **130**, 5452–5458.

(18) T. Ghosh, B. M. Leonard, Q. Zhou and F. J. DiSalvo, *Chem. Mater.* 2010, **22**, 2190–2202.

(19) T. Ohsawa, Y. Adachi, I. Sakaguchi, K. Matsumoto, H. Haneda, S. Ueda, H. Yoshikawa, K. Kobayashi and N. Ohashi, *Chem. Mater.* 2009, **21**, 144–150.

(20) D.H. Chun, Y. Xu, M. Demura, K. Kishida, D.M. Wee and T. Hirano, *J. Catal.* 2006, **243**, 99–107.

(21) P. J. Perdew, K. Burke and M. Ernzerhof, *Phys. Rev. Lett.* 1996, **77**, 3865–3868.

(22) G. Kresse and J. Furthmüller, *Phys. Rev. B* 1996, **54**, 11169–11186.

(23) G. Kresse and J. Hafner, *Phys. Rev. B* 1993, **47**, 558–561.

(24) *Pearson's Handbook of Crystallographic Data for Intermetallic Phases*; P. L. Villars, L. D. Calvert, Eds.; American Society for Metals: Metals Park, OH, 1985; Vol. **3**, pp 3044, 3058, 3059.

(25) B.C. Giessen, R.H. Kane and N.J. Grant, *Trans. Metall. Soc. AIME* 1965, **233**, 855–864.

(26) A. E. Dwight and P. A. Beck, *Trans. Metall. Soc. AIME*, 1959, **215**, 976–979.

(27) B. Hammer, Y. Morikawa, J. K. Nørskov, *Phys. Rev. Lett.* 1996, **76**, 2141–2144.

(28) A. Dauscher, L. Hilaire, J. C. Spirlet, W. Müller and G. Maire, *Surf. Sci.* 1988, **204**, 161–173.

(29) G. N. Derry and P. N. Ross, *Solid State Commun.* 1984, **52**, 151–154.

(30) W. Chen, L. Severin, M. Göthelid, M. Hammer, S. Cameron,; J. Paul, *Phys. Rev. B.* 1994, **50**, 5620–5627.

(31) A. R. Burke, C. R. Brown, W. C. Bowling, J. E. Glaub, D. Kapsch, C. M. Love, R. B. Whitaker and W. E. Moddeman, *Surf. Interface Anal.* 1988, **11**, 353–358.

(32) R. P. Netterfield, P. J. Marin, C. G. Pacey, W. G. Sainty, D. R. McKenzie and G. Auchterlonie, *J. Appl. Phys.* 1989, **66**, 1805–1809.

(33) J. D. Rogers, V. S. Sundaram, G. G. Kleiman, C. G. C. Castro, R. A. Douglas, A. C. Peterlevitz, *J. Phys. F* 1982, **12**, 2097–2102.

(34) S. F. Ho, S. Contarini and J. W. Rabalais, *J. Phys. Chem.* 1987, **91**, 4779–4788.

(35) C. Morant, L. Galán and J. M. Sanz, *Surf. Interface Anal.* 1990, **16**, 304–308.

(36) P. Légaré, G. Lindauer, L. Hilaire, G. Maire, J. J. Ehrhardt, J. Jupille, A. C. Cassuto, Guillot and J. Lecante, *Surf. Sci.* 1990, **198**, 69–78.

(37) J. Paul, S. D. Cameron, D. J. Dwyer and F. M. Hoffmann, *Surf. Sci.* 1986, **177**, 121–138.

(38) W. Chen, E. Chulkov and J. Paul, *Physica Scripta* 1996, **54**, 392–396.

(39) J. A. Rodriguez and D. W. Goodman, *Science* 1992, **257***,* 897–903.

(40) J. A. Rodriguez, C. M. Truong, D. W. Goodman, *J. Chem. Phys.* 1992, **96**, 7814–7825.

(41) P. N. Ross, *J. Vac. Sci. Technol.* 1992, **A10**, 2546–2550.

(42) P. N. Ross, *Electrochim. Acta* 1991, **36**, 2053–2062.

(43) U. Bardi, D. Dahlgren and P. N. Ross, *J. Catal.* 1986, **100**, 196–209.

(44) U. Bardi, G. A. Somorjai and P. N. Ross, *J. Catal.* 1984, **85**, 272–276.

(45) T. Jiang , D. J. Mowbray, S. Dobrin, H. Falsig, B. Hvolbæk, T. Bligaard and J. K. Nørskov, *J. Phys. Chem. C,* 2009, **113**, 10548–10553.

TOC

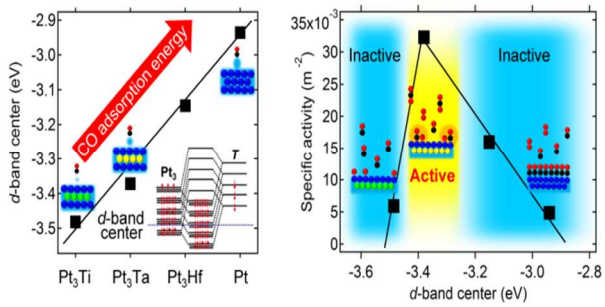

The CO-oxidation activity of Pt and Pt alloys, Pt3T (T = Ti, Hf, Ta, Pt), shows a volcano-type dependence on the d-band center of the catalysts.